Journal of Constructional Steel Research 186 (2021) 106915

Contents lists available at ScienceDirect

Journal of Constructional Steel Research

journal homepage: www.elsevier.com/locate/jcsr

Utilizing an I-shaped shear link as a damper to improve the behaviour of a concentrically braced frame

Ali Ghamari [a,b], Young-Ju Kim [c], Jaehoon Bae [d,*]

[a] Department of Civil Engineering, Darreh Shahr Branch, Islamic Azad University, Darreh Shahr, Iran
[b] Futurology Research Center in Science and Technology, Ilam Branch, Islamic Azad University, Ilam, Iran
[c] Korea Institute of Structural Engineering & Consulting, Busan, Republic of Korea
[d] Department of Architecture, Chonnam National University, 50 Daehak-ro Yeosu-si, Jeonnam 59626, Republic of Korea

ARTICLE INFO

Keywords:
I-shaped
Shear
Ultimate strength
Over-strength
Yielding
Concentrically braced frames

ABSTRACT

Over the past few decades, concentrically braced frames (CBFs) have become a commonly used load-resistant bearing system in steel structures. CBF systems have high lateral stiffness and lateral strength; however, they have low ductility and a low seismic energy dissipating capacity. Under seismic loading, the diagonal elements of a CBF system are susceptible to buckling, causing hysteresis in the compression zone and severely reducing energy absorption. Although steel dampers improve the hysteretic behaviour of the braces, they impose additional costs on structures. Therefore, in this study, an I-shaped steel damper with a shear yield mechanism was introduced; this is an economical solution, has a simple construction, and can be easily replaced after an earthquake. The proposed damper was evaluated numerically and parametrically. Results indicate that the proposed damper acts as a ductile fuse that prevents buckling of the diagonal element of a CBF system. It was found that both the web and flange plates contribute to the shear resistance, with the flange carrying approximately 15% of the shear force, as expressed in the presented equations. Additionally, overstrength obtained for the damper was greater than 1.5 (proposed by AISC). Necessary relations are represented to predict and design the damper and the elements outside it.

1. Introduction

A concentrically braced frame (CBF) system is a lateral resisting system that has high lateral strength and stiffness in comparison with other conventional systems such as eccentrically braced frame (EBF) system and moment resisting frame (MRF) system. However, CBF systems have a low seismic energy dissipating capacity. The buckling of CBF diagonal elements under compression loading leads to degradation of the lateral stiffness and strength of the system. Therefore, the system does not exhibit ductile behaviour under seismic loading. Over the past decades, the EBF system has been introduced as a ductile system in seismic zones. The ductile performance of the system depends on link segments. The link length, e, is a key parameter in EBF systems that affects the mechanism, stiffness, strength, and ductility. The mechanism of the system is categorised by the link-length ratio, $\rho = e/(M_P/V_P)$, where M_P and V_P are the plastic moments and plastic shear capacities of the link, and it provides a convenient measure for yield behaviour. The mechanism of the link is measured with $\rho < 1.6$, $\rho > 2.6$ for shear yielding and flexural yielding mechanisms respectively. Extensive data reported by Hjelmstad and Popov [1], Malley and Popov [2], Kasai and Popov [3], Popov and Engelhardt [4,5], Okazaki et al. [6–8] have indicated that a properly detailed shear link can provide stable, ductile and predictable behaviour under cyclic loading.

In a conventional EBF system, the link beam is horizontal and is a part of the floor beam [9]. The EBF system with a horizontal link beam is a well-known structural system among researchers; this favourability is based on experimental and numerical reports. Comprehensive studies have been performed on the seismic performance and design of conventional EBF systems over the past decades. The need for replacing story beams after severe earthquakes and deformation of the slabs due to link rotations, is the main drawback of this structural system [10]. In a conventional EBF system with horizontal links, considerable axial forces develop, which should be included in the seismic design and analysis process [11,12]. When a horizontal link is attached to the column, its axial force imposes considerable shear force on the column. Several studies have attempted to improve conventional EBF by using

* Corresponding author.
E-mail addresses: aghamari@alumni.iust.ac.ir (A. Ghamari), skycity-bjh@jnu.ac.kr (J. Bae).

https://doi.org/10.1016/j.jcsr.2021.106915
Received 2 April 2021; Received in revised form 22 July 2021; Accepted 10 August 2021
Available online 21 August 2021

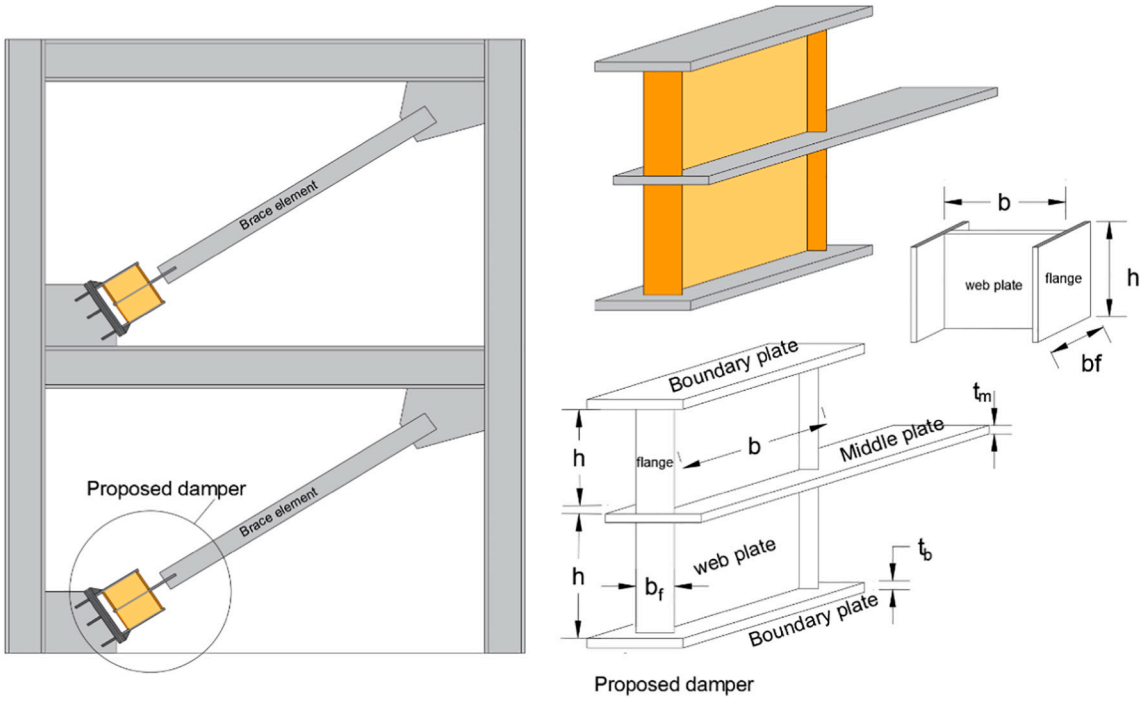

Fig. 1. Proposed damper

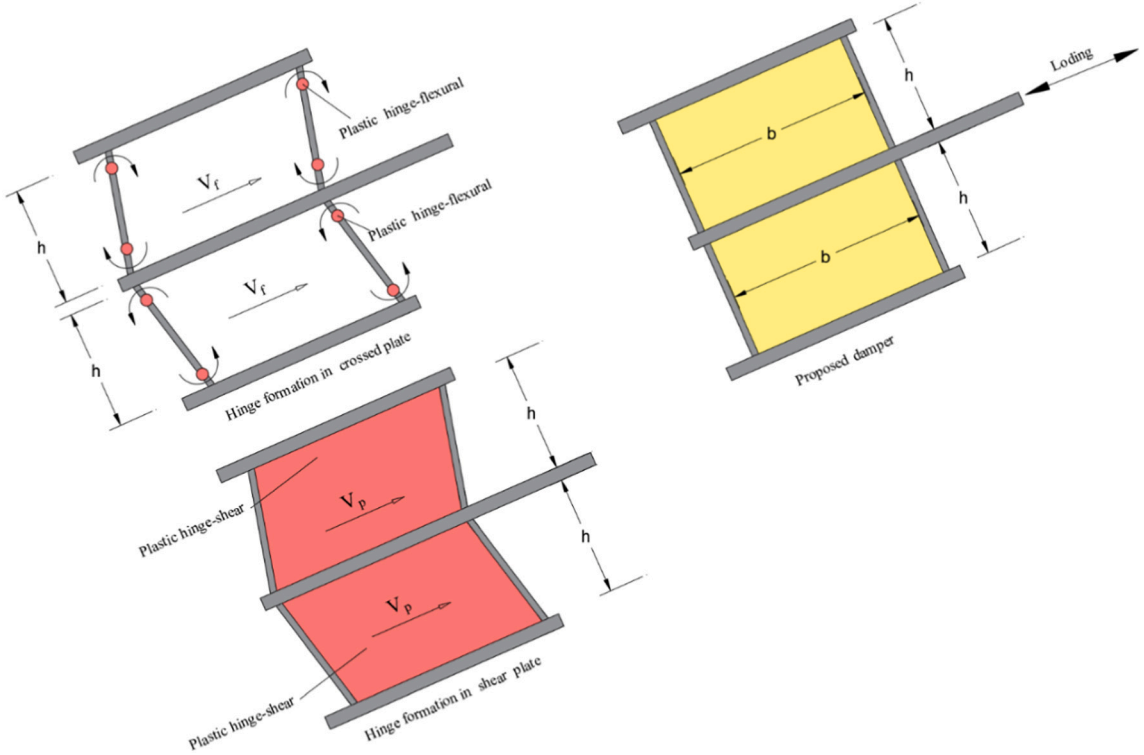

Fig. 2. Hinge formation over the shear damper

replaceable link beams [13,14].

Using a vertical shear link in the EBF system (V-EBF), the need for replacement after a severe earthquake can be resolved [15]. In this system, the link segments are attached under the floor beam, between the floor beam and brace members, which are not under axial load. In the other words, the effects of the axial force in the vertical links are negligible. Further, unlike conventional EBF systems, the floor beam and slabs are not affected by link rotation. This V-EBF system was developed by Seki [16] as an efficient lateral resist system. The stable hysteretic curves and high energy dissipation capacity are presented as the most notable features of this system [17–19]. The vertical links act as a ductile fuse, and the majority of the imposed seismic energy is absorbed by them. The seismic ductile fuse limits the damage in the link, and the other structural members remain elastic [20]. The main weakness of the

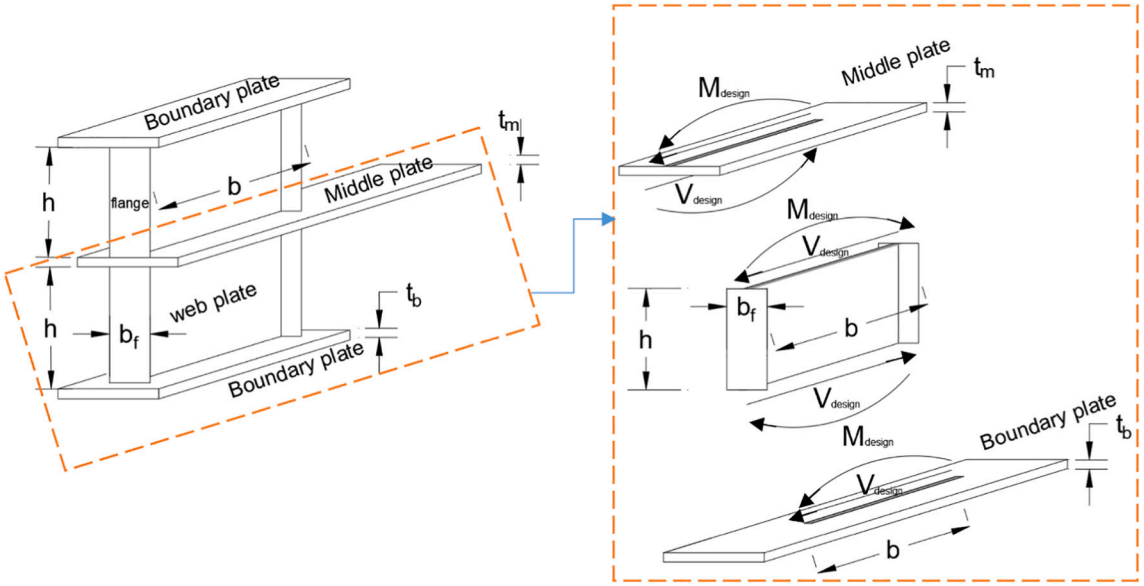

Fig. 3. Free body diagram for the design of boundary plates

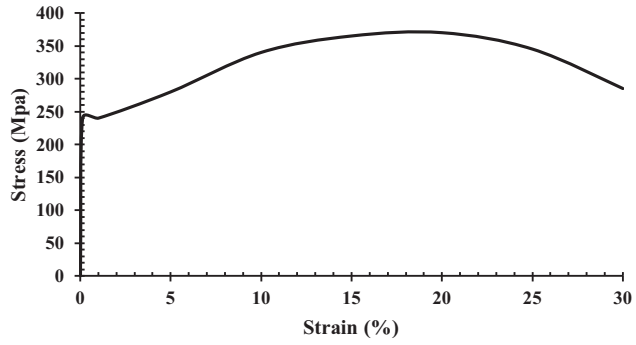

Fig. 4. Stress-strain curve of ST37 steel.

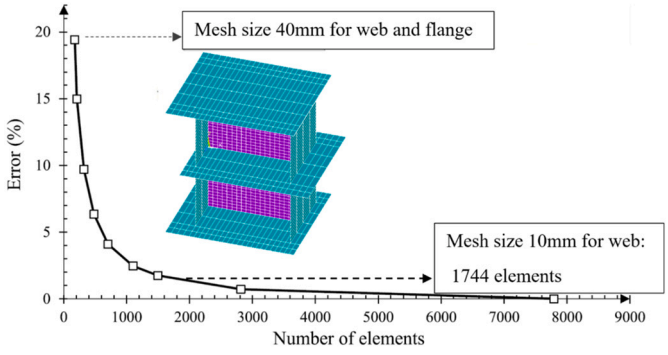

Fig. 5. FE modelling; meshing and mesh sensitivity

system is that the system stiffness is less than that of a conventional EBF system [21].

In this study, a shear link is used as a replaceable segment attached to the end of the CBF diagonal element. The replaceable segment (proposed damper) acts as the ductile fuse that limits damages to the damper. The ductile behaviour of the proposed shear damper prevents the buckling of the CBF diagonal element. Preventing its buckling takes the CBF system from a brittle mechanism (buckling) to a ductile mechanism (yielding of the damper). The proposed damper is designed such that it is easy to construct. Due to the ease of fabrication of the proposed damper and its low cost of construction, it does not result in significant additional costs for the overall structure. Thus, its use is justified from an economic point of view. In this study, the behaviour of the proposed damper is investigated numerically and parametrically. In addition, equations required for the design of the damper are proposed.

2. Proposed shear damper

2.1. Fabrication of the shear damper

The proposed shear damper consists of the main plate as a web, and two end flange plates that give the damper an I-shaped form. The damper is attached at the end of the diagonal CBF element as shown in Fig. 1. This design can be implemented easily. Either pin or rigid beam-to-column connections can be used for a CBF system equipped with the damper. When pin beam-to-column connections are used, the entire lateral load is resisted by the damper.

2.2. Ultimate strength of the shear damper

Based on the AISC 341-16 [22] regarding I-section links, the shear capacity is calculated using Eq. (1). Article F3.5b.2 of the AISC 341-16 determines the design shear strength, $\phi_v V_n$, in which ϕ_v is the shear resistance coefficient. For an I-shaped shear link, it is calculated by $V_n = V_P$ where the V_p is calculated using Eq. (1). Furthermore, for an I-shaped link with a flexural mechanism, the strength is determined as $V_n = 2M_P/e$. Another point of interest is the alternative definition of V_P in certain AISC360-16 [23] specifications that replace h with d, where d is girder depth and $h = d - 2t_f$. Here, t_f is the thickness of the flange. It should be noted that h in AISC equals b in the proposed damper.

$$V_p = 0.6F_{yw}bt_w \tag{1}$$

This study is carried out under the assumption that shear loading is applied not only to the web plate, but also to the flange plate. Since two I-shaped dampers are used for constructing the damper, a coefficient 2 is multiplied.

$$V_n = 2(V_p + V_f) \tag{2}$$

where V_f,is the shear strength of the flange plate.

AISC specifications recommend calculating the nominal shear ca-

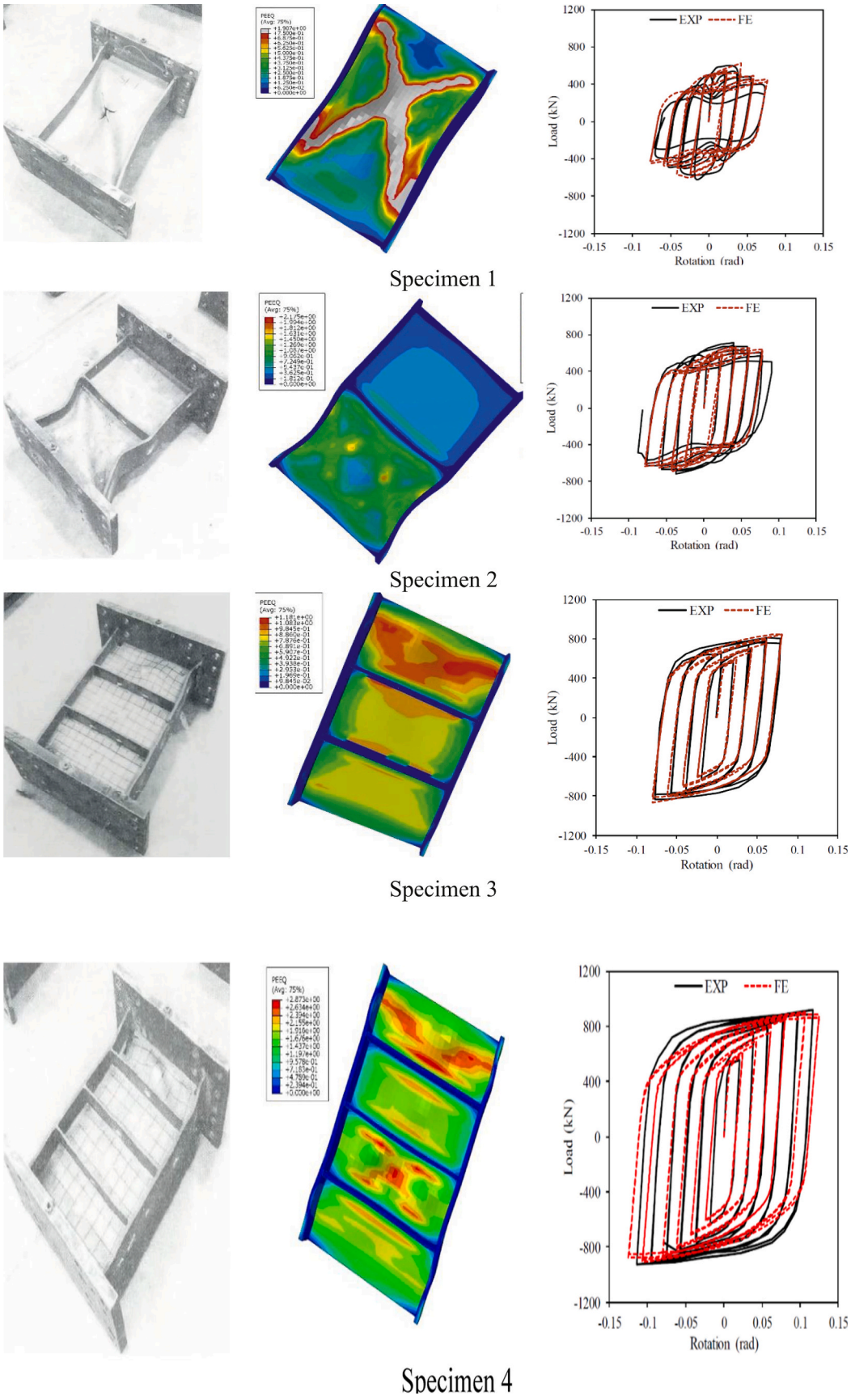

Fig. 6. Comparing FE simulation results with experimental results

Table 1
Properties of the models for Parametrical study.

Model	h (mm)	t_w (mm)	t_f (mm)	b_f (mm)	b (mm)	Eq. (10a)	Eq. (10b)	ρ	ψ
140-10-0.25-6.3	140	6	10	160	200	33	8	0.25	6.30
140-15-0.18-2.8	140	6	15	160	200	33	5	0.18	2.80
140-20-0.13-1.58	140	6	20	160	200	33	4	0.13	1.58
140-25-0.11-1.00	140	6	25	160	200	33	3	0.11	1.01
140-30-0.10-0.7	140	6	30	160	200	33	3	0.09	0.70
210-10-0.38-9.45	210	6	10	160	200	33	8	0.38	9.45
210-115-0.26-4.2	210	6	15	160	200	33	5	0.26	4.20
210-20-0.2-2.36	210	6	20	160	200	33	4	0.20	2.36
210-250-0.16-1.51	210	6	25	160	200	33	3	0.16	1.51
210-30-0.13-1.05	210	6	30	160	200	33	3	0.13	1.05
280-10-0.51-12.6	280	6	10	160	200	33	8	0.51	12.60
280-15-0.35-5.6	280	6	15	160	200	33	5	0.35	5.60
280-20-0.26-3.15	280	6	20	160	200	33	4	0.26	3.15
280-25-0.21-2.02	280	6	25	160	200	33	3	0.21	2.02
280-30-0.17-1.4	280	6	30	160	200	33	3	0.17	1.40
350-10-0.64-15.75	350	6	10	160	200	33	8	0.64	15.75
350-15-0.44-7.0	350	6	15	160	200	33	5	0.44	7.00
350-20-0.33-3.94	350	6	20	160	200	33	4	0.33	3.94
350-25-0.26-2.52	350	6	25	160	200	33	3	0.26	2.52
350-30-0.22-1.75	350	6	30	160	200	33	3	0.22	1.75

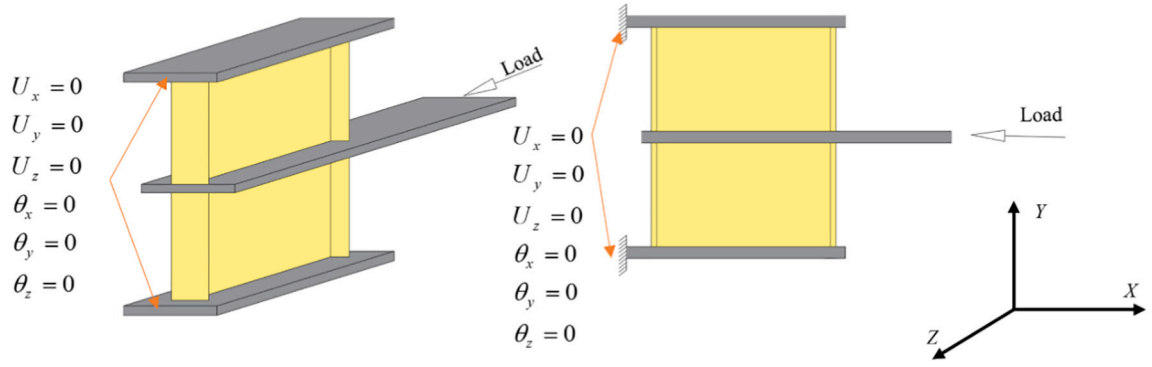

Fig. 7. Boundary conditions.

pacity of short links based on the web area without including the contribution of the flanges. However, according to the findings of McDaniel et al. [24], in short links, the flanges are also subject to significant shear loading. Manheim and Popov [25] and Richards [26] proposed that the flange effect should be considered in determining the plastic shear capacity of the link. Since shear loading is also applied to the flanges, Eq. (3) is proposed to account for the same.

$$V_p = \eta 0.6 F_{yw}\left(b + 2t_f\right)t_w \tag{3}$$

In this equation, to consider the effect of strain hardening, it is proposed that η be equal to 1.1. The upper bound for the equation can be found when four flexural plastic hinges are formed in the flange plates, as illustrated in Fig. 2. Hinges are formed when the moment reaches plastic moment. To satisfy equilibrium conditions, Eq. (4) must hold.

$$V_f = \frac{4M_{pf}}{h}, \tag{4}$$

where M_{pf} is the plastic moment of the flange plate, and it is calculated as $M_{pf} = \frac{b_f t_f^2}{4} F_{yf}$; F_{yf} is the yielding stress of the flange plate. Other parameters have been introduced in Fig. 1.

The damper is expected to yield before nonlinear behaviour occurs in the diagonal element of the brace. In other words, the nonlinear behaviour in the damper is limited and the diagonal element remains elastic. Regarding the nonlinear behaviour of the damper, one may expect the formation of a shear plastic hinge in the web plate, and the formation of a bending hinge at both ends of the flange plate.

2.3. Design of the diagonal element equipped by the shear damper

Under lateral loading, it is expected that inelastic behaviour is limited to the damper while elements outside the damper remain elastic. To achieve this behaviour, the damper should yield before other elements of the structures. To that end, the proposed damper is designed based on Eq. (5). The shear in the damper is produced by the axial force in brace N, where N is the axial force in the brace. The value of N is determined as $N = \frac{V}{cos\alpha}$, where V is the lateral shear applied to the structure and α is the angle of the diagonal element of the brace relative to the horizontal line.

$$N \le \phi V_n, \tag{5}$$

where $\phi = 0.9$ and $V_n$is calculated using Eq. (2). Eq. (5) is based on the assumption that the beam-column connection is the pin, and the diagonal bracing consequently takes all the shear force. If the beam-column connection is rigid, the lateral load is distributed between the frame and the brace based on their stiffness. Elements outside of the damper are optimized for the maximum subject to Eq. (6).

$$V_{design} = 1.25 R_y V_n, \tag{6a}$$
$$V_{design} = \Omega_0 V_n. \tag{6b}$$

where $\Omega_0$is the over-strength that is considered in the next sections.

To maintain the damper as a ductile fuse, the diagonal element should be designed based on the maximum strength of the damper, based on Eq. (6). Therefore, the following inequality should be satisfied:

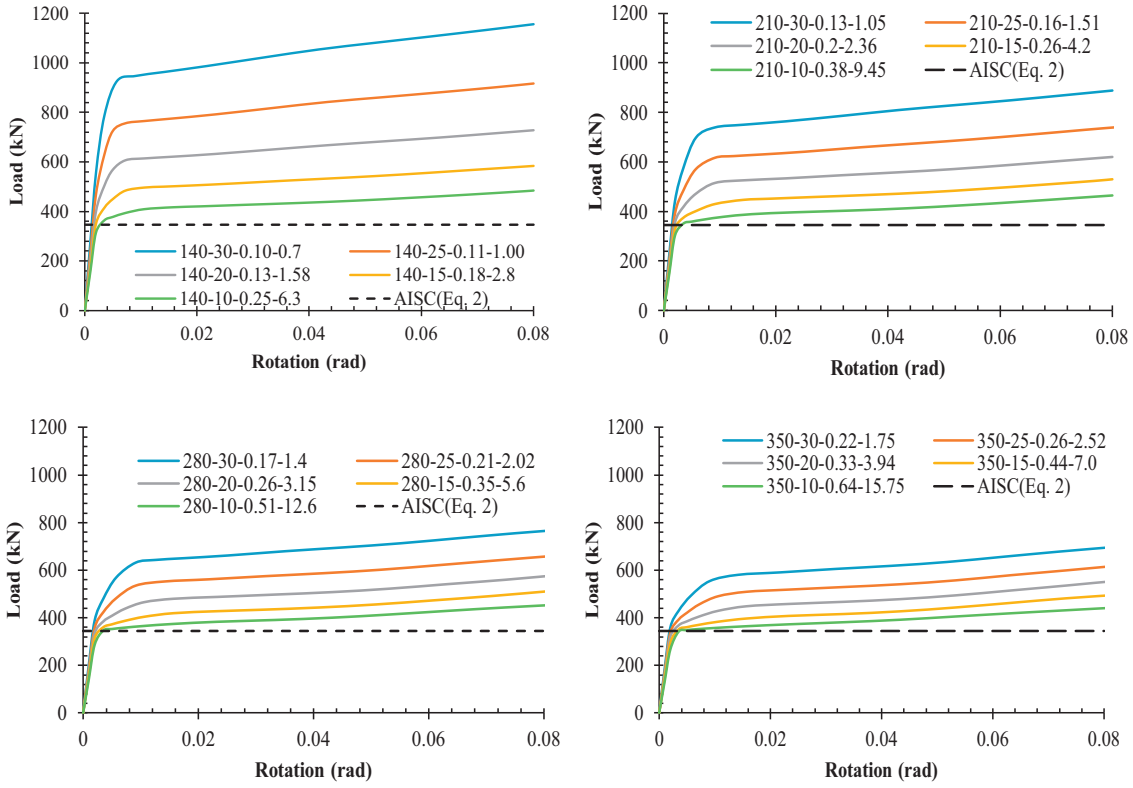

Fig. 8. Load-rotation curves of FE simulation models.

$$V_{design} \leq \Phi P_n, \tag{7}$$

where V_{design} is the design force, Φ is the compressive strength reduction coefficient (equal to 0.9), and P_n is the nominal compressive strength of the compression members according to AISC 360-16 [23], which are calculated from the following equation:

$$P_n = \left(0.658^{\frac{F_y}{F_e}}\right) F_y A, \lambda \leq 4.71\sqrt{\frac{E}{F_y}} \tag{8a}$$

$$P_n = 0.877 F_e A, \lambda > 4.71\sqrt{\frac{E}{F_y}} \tag{8b}$$

where λ is the slenderness ratio $\lambda = \frac{KL}{r}$. In this relation, the coefficient K is the effective length L factor. Further, r and A are the radius of gyration and gross area of cross-section of the diagonal element, respectively. Here, F_y gives the specified minimum yield stress, E refers to the modulus of elasticity, and the F_e is the buckling stress of the diagonal element, and is determined to be:

$$F_e = \frac{\pi^2 E}{\lambda^2} \tag{9}$$

If the beam-to-column connection is of the pin type, all lateral load is carried by the damper.

The boundary plate also is designed under V_{design}. A weak boundary plate may reduce the ultimate strength and dissipating energy of the main plate (web plate). With a weak boundary plate, yielding does not develop entirely in the web plate.

Fig. 3 illustrates the free body diagram to derive forces for the design of boundary plates. The boundary elements are affected by V_{design} and M_{design} where they are, respectively, amplified shear force and amplified bending moment of the damper. The value of V_{design} is obtained from Eq. (6) and M_{design} is obtained through the relation $M_{design} = V_{design}h$. The boundary plate should be designed to resist the forces corresponding to V_{design} and M_{design}.

3. Numerical study

3.1. Modelling

In this study, ANSYS was utilized to simulate finite element (FE) models. To this end, SHELL 181 was used with 4 nodes, accounting for 6 degrees of freedom in each node. This element design can admit large displacement, buckling, and material nonlinearity.

In the FE modelling, for all elements, ST37 steel was used with yield stress and ultimate stress of 240 and 370 MPa, respectively. Further, the ST37 steel has a Poisson's ratio of 0.3 and a Young's modulus of 200 GPa. Fig. 4 illustrates the stress-strain curve of ST37 steel.

Both nonlinearities (materials and geometry) were measured in this study. Material nonlinearity was considered by defining the stress-strain relationship of the material. The geometry nonlinearity was considered by applying imperfection. To measure the imperfection, buckling analysis was first performed; then the FE model was updated considering the reformatted model based on the buckled model. As a result, the first positive eigenmode of each link was amplified by a magnitude of h/10000, which is then used as the initial shape for nonlinear analysis. The magnitude of h/10000 was selected based on the finding of Ref [19]. Fig. 6 shows the FE simulation of a schematic model and mesh sensitivity analysis. In this figure, the error was considered the difference between the buckling stress determined in the model with the given mesh and the buckling stress obtained in the model with the highest considered number of elements.

Some analysis was carried out to achieve the optimal extent of meshing, as shown in Fig. 5. The optimal mesh was obtained with an error of 2.5%.

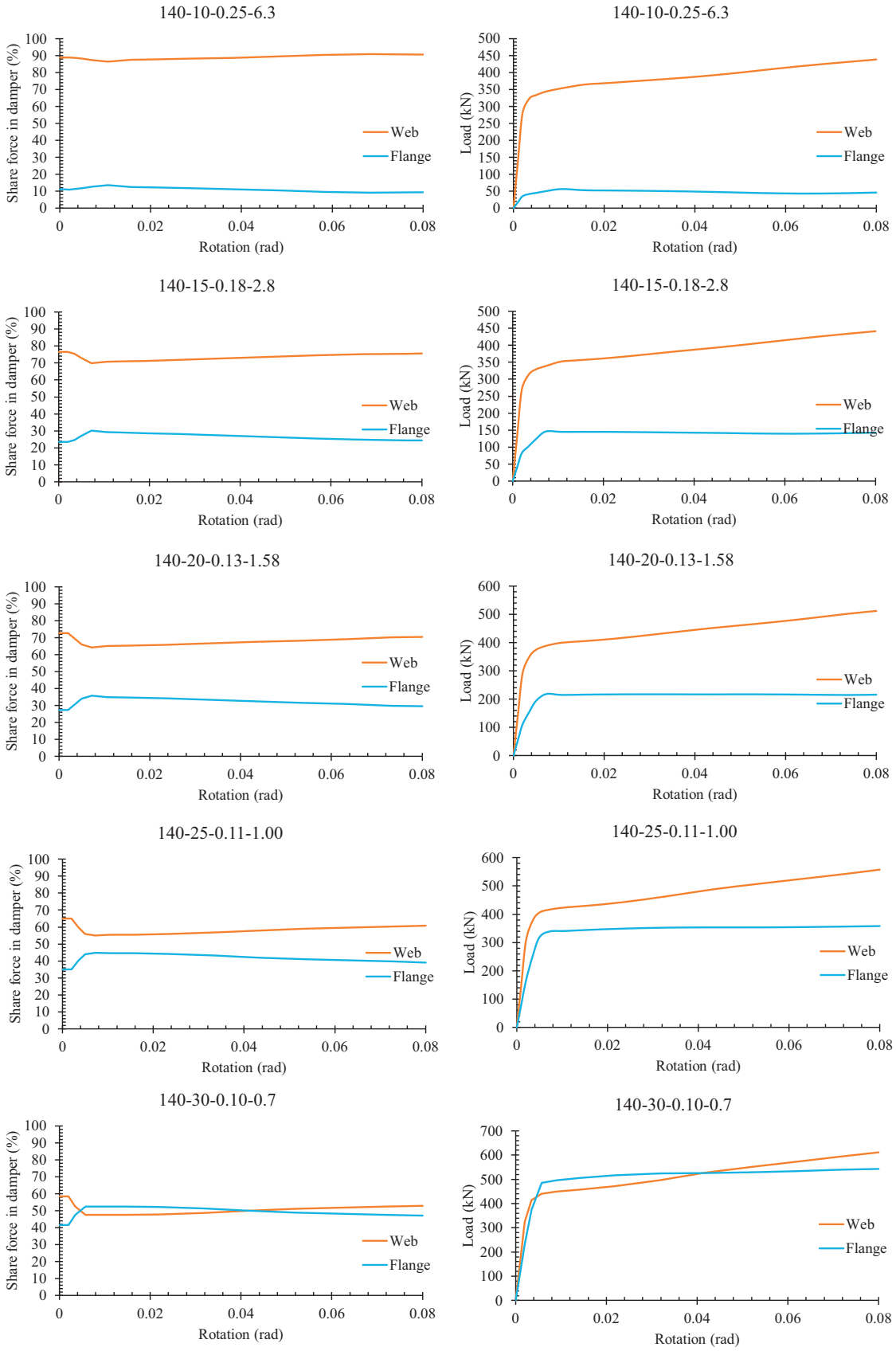

Fig. 9. The percentage share of load for the shear damper with h = 140 mm.

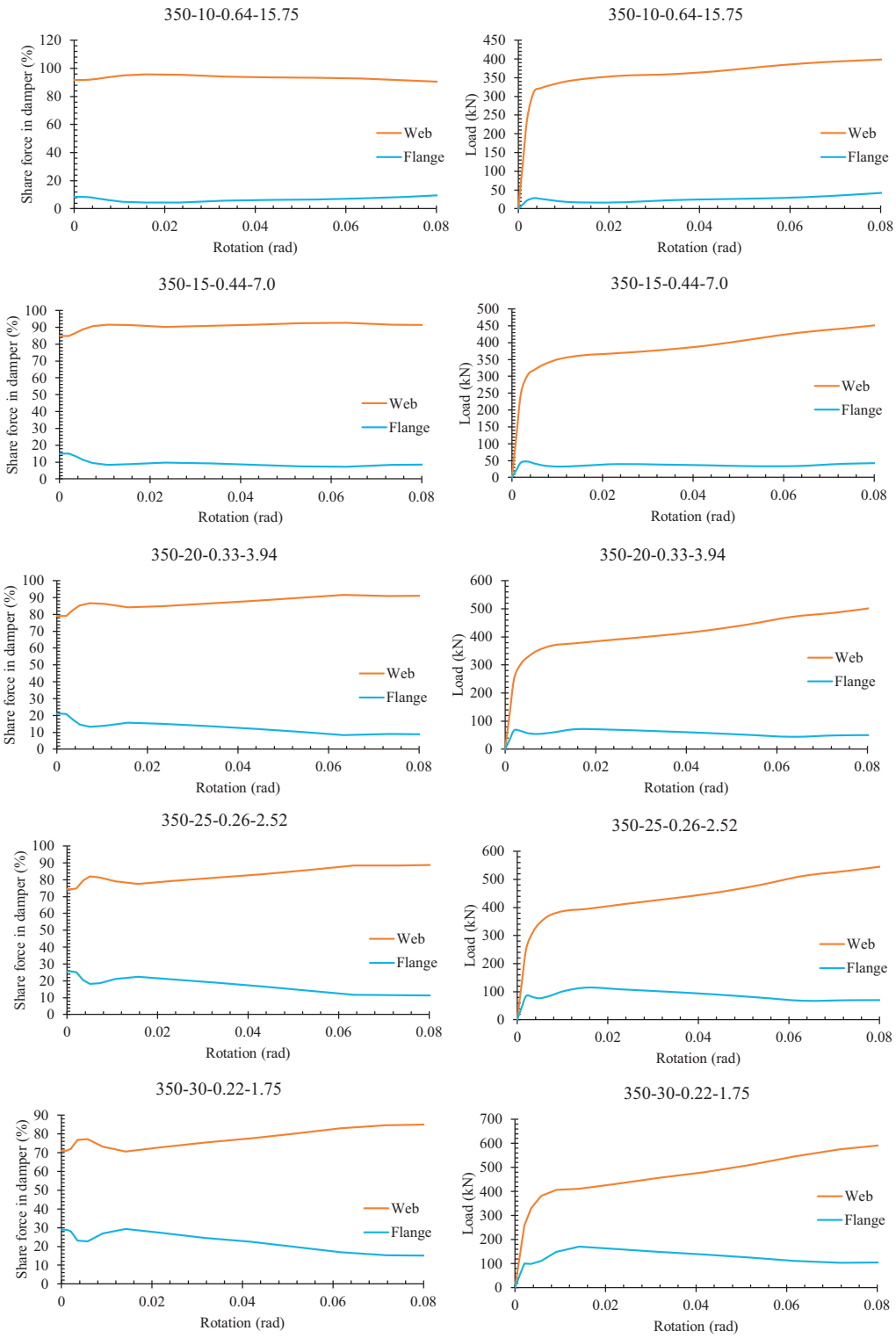

Fig. 10. The percentage share of load for the shear damper with h = 350 mm

3.2. Verification of FE results

Four experimental specimens tested by Hjelmstad and Popov [1] were used to verify the FE simulation results. The link length ratio for all specimens was equaled to 1.13. These specimens were made of W18 × 40, with length 711 mm, and A36 materials. Specimen 1 was taken without stiffeners, and a stiffener was placed in the middle of Specimen 2. For Specimens 3 and 4, two and three stiffeners were used respectively, as shown in Fig. 7. The links are shear elements with boundary stiffeners that act as the proposed damper. Subsequently, the same

Table 2
Contribution of the flange to the load resistance of the damper.

b/h	Models	t_f (mm)	ρ	ψ	min (%)	max (%)
0.7	140-10-0.25-6.3	10	0.25	6.30	9.16	13.67
	140-15-0.18-2.8	15	0.18	2.80	23.39	30.09
	140-20-0.13-1.58	20	0.13	1.58	27.34	35.85
	140-25-0.11-1.00	25	0.11	1.01	34.95	44.89
	140-30-0.10-0.7	30	0.09	0.70	41.60	52.53
1.05	210-10-0.38-9.45	10	0.38	9.45	6.66	9.79
	210-15-0.26-4.2	15	0.26	4.20	10.84	16.87
	210-20-0.2-2.36	20	0.20	2.36	6.66	9.79
	210-25-0.16-1.51	25	0.16	1.51	6.66	9.79
	210-30-0.13-1.05	30	0.13	1.05	6.66	9.79
1.40	280-10-0.51-12.6	10	0.51	12.60	5.95	9.02
	280-15-0.35-5.6	15	0.35	5.60	7.95	15.94
	280-20-0.26-3.15	20	0.26	3.15	5.95	9.02
	280-25-0.21-2.02	25	0.21	2.02	5.95	9.02
	280-30-0.17-1.4	30	0.17	1.40	5.95	9.02
1.75	350-10-0.64-15.75	10	0.64	15.75	4.43	9.98
	350-15-0.44-7.0	15	0.44	7.00	7.33	15.10
	350-20-0.33-3.94	20	0.33	3.94	4.43	9.98
	350-25-0.26-2.52	25	0.26	2.52	4.43	9.98
	350-30-0.22-1.75	30	0.22	1.75	4.43	9.98

Table 3
Comparison of ultimate strength of FE simulation models.

Models	ρ	ψ	t_f (mm)	Vu (kN)	$\frac{V_{u(i)}}{V_{u(h=140mm)}}$	$\frac{V_{u(i)}}{V_{u(t_f=10mm)}}$
140-10-0.25-6.3	0.25	6.30	10	484.76		
140-15-0.18-2.8	0.18	2.80	15	583.88		1.20
140-20-0.13-1.58	0.13	1.58	20	727.55		1.25
140-25-0.11-1.00	0.11	1.01	25	917.02		1.26
140-30-0.10-0.7	0.09	0.70	30	1155.30		1.26
210-10-0.38-9.45	0.38	9.45	10	465.46	0.96	
210-15-0.26-4.2	0.26	4.20	15	530.31	0.91	1.14
210-20-0.2-2.36	0.20	2.36	20	620.16	0.85	1.17
210-25-0.16-1.51	0.16	1.51	25	749.37	0.82	1.21
210-30-0.13-1.05	0.13	1.05	30	888.29	0.77	1.19
280-10-0.51-12.6	0.51	12.60	10	455.72	0.94	
280-15-0.35-5.6	0.35	5.60	15	511.02	0.88	1.12
280-20-0.26-3.15	0.26	3.15	20	581.32	0.80	1.14
280-25-0.21-2.02	0.21	2.02	25	661.21	0.72	1.14
280-30-0.17-1.4	0.17	1.40	30	773.43	0.67	1.17
350-10-0.64-15.75	0.64	15.75	10	444.70	0.92	
350-15-0.44-7.0	0.44	7.00	15	498.51	0.85	1.12
350-20-0.33-3.94	0.33	3.94	20	573.63	0.79	1.15
350-25-0.26-2.52	0.26	2.52	25	621.87	0.68	1.08
350-30-0.22-1.75	0.22	1.75	30	698.29	0.60	1.12

boundary conditions and mechanisms are applicable in the experimental test and for the proposed damper.

In the experimental test, the plate located at the bottom of the link was bolted to a rigid beam. The top plate was bolted to a beam and lateral loads were applied to the plate. To simulate the fixed condition of the bottom plate, nodes of the bottom plate were restrained from displacement and rotation in all directions. To simulate the boundary condition of the top plate, nodes of the top plate were restrained from rotation in all directions. However, the out-of-plane displacements of the top plate were also restrained. The nodes were free from displacement along the loading direction.

Comparison of FE simulation results with the experimental test, Fig. 6, in case of deformation and hysteresis curves, reveals a good accuracy of the FE simulation. The comparisons show that the FE simulation results are matched with experimental test results in the elastic zone. Also, FE results measure the ultimate strength of the test with a maximum error of 4.5%.

4. Parametrical study

4.1. Details of parametrical models

For the parametric study of the behaviour of the proposed damper, the FE models were designed as listed in Table 1. The name of each model indicates the values used for the parameters (h-t_f-ρ-ψ). For all models, the parameters b and t_w were kept constant at 200 and 6 mm, respectively. This gives a fair comparison between the FE models. The variables considered for the parametric study are the coefficients ρ and ψ. The parameter ψ is defined as $\psi = \frac{V_p}{V_f}$. As per F3.5b of the AISC341-16, shear links should satisfy the requirements of section D1.1 [22] for highly ductile elements (which was considered for the models of this article according to Table 1.). In this standard, flanges of I-shaped shear links ($\rho \leq 1.6$) are permitted to satisfy the supplies for moderately ductile members. In table D1.1 of the AISC341-16 [22], the ratios $\frac{d-2t_f}{t_w}$ (width to thickness of the web) and $\frac{b_f}{2t_f}$ (free width to thickness of the flange) of I-shaped links are defined as follows:

$$\frac{d-2t_f}{t_w} \leq 1.57\sqrt{\frac{E_w}{R_{yw}F_{yw}}}\ (\text{Highly ductile elements}), \tag{10a}$$

$$\frac{b_f}{2t_f} \leq 0.40\sqrt{\frac{E_f}{R_{yf}F_{yf}}}\ (\text{Moderately ductile elements}), \tag{10b}$$

where, E_w and E_f are the Young's modulus of the web and flange plates, respectively; R_{yw} and R_{yf} are the ratios of the expected yield stress of the web and flange plates to the specified minimum yield stress, respectively. The values of R_y are reported in Table A3.1 of the AISC341-16 [22] in detail, for various steel and steel reinforcement materials. The parametrical models were designed to satisfy the equations.

4.2. Boundary conditions and materials

The behaviour of the shear damper was examined under boundary conditions as shown in Fig. 7. To impose the fixed support at the location of the damper attached to the gusset plate, all degrees of freedom were restricted. At the other end of the damper, where the diagonal element is attached to the damper, loading was applied. The loading is displacement control; it is increased until the amount of drift (rotation) reaches 8% (0.08 rad). As pointed out in article F3.4a of the AISC 341-16 [23], short/shear links attain a maximum rotation of 0.08 rad under seismic loading. Therefore, for models with h = 140, 210, 280, and 350 mm, the

displacement was determined to be 11.2, 16.8, 22.4, and 28 mm, respectively. Since the response of shear links is symmetric, monotonic loading was applied to reduce analysis time. Cyclic loading was applied only for diagonal elements equipped with the damper, based on the ATC24. The rationale behind the application of cyclic loading is to investigate the capacity of the damper to act as a ductile fuse.

5. Results and discussion

5.1. Load-displacement curves

Fig. 8 illustrates the load-rotation of the FE simulation models. This figure contains an important finding that is considered subsequently. In this section, we discuss methods to enhance the overall behaviour of the system. Based on the AISC, when $\rho < 1.6$ shear yielding is governed by link behaviour; for the I-shaped link, its ultimate strength is determined by Eq. (2). Referring to Fig. 7, Eq. (2) attributes minimum ultimate strength for the FE simulation models. However, when ρ is decreased beyond 1.6, the behaviour of the link changes in a manner that has not been documented in the AISC341-16 [22].

Although bt_wvalues for the FE simulation models are the same, with $\rho < 1.6$, they exhibit different load-rotations (with different ultimate strength, over-strength, and energy absorption). Therefore, it is necessary to achieve a larger ultimate strength for elements outside the link than link; this is outlined in Section 7.

5.2. Share of the flange in shear capacity

An alternative method to evaluate the effectiveness of flanges is to measure the amount of absorbed load. Figs. 9 and 10 illustrate the contribution shares of the flanges and webs of the shear damper with h = 140 mm, having different t_f and ψ values across its loading history. To summarise the results, models with h = 140 and 350 mm were considered; the results are listed in Table 2. Upon the formation of a shear hinge in the web plate, the plates begin to lose their effectiveness and frames become more active up to rotations of 0.08 rad. After a rotation of 0.01 rad, the share of both flange and web plates tends to be constant. The figures and table show that the flange absorbs a high percentage of the load when flange thickness is increased, for the case when b/h is less than 1. For b/h > 1, the flange absorbs 4% to 15% of the imposed load, which is not negligible.

5.3. Effect of the flange on the ultimate strength of the damper

The ultimate strength of the models is shown in Table 3. By increasing h, ultimate strength is reduced for all models when $\rho < 1.6$. For dampers with $t_f = 10$ mm and 30 mm, ultimate strength is reduced for different *h* values, by 4% to 8% and 23% to 40%. Therefore, the reduction of V_u is higher for dampers with higher t_f. By increasing t_f while keeping h constant, ultimate strength increases from 8% to 26%. One can conclude that ultimate strength of the damper is not only related to ρ and ψ, but also to t_f and h. Therefore, by increasing t_f, V_u is raised by at least 8%; a new relation is needed to measure the ultimate strength of the damper, especially for the design of the element outside the link.

5.4. Over-strength of the shear damper

In this section, the over-strength, Ω_0, is considered. Although in the AISC341-16, Ω_0 is assumed to be constant for each structure, researchers [27] showed that $\Omega_0$it is not constant for I-shaped links under shear loading. The over-strength is calculated using Eq. (11).

$$\Omega_0 = \frac{V_u}{V_s}, \tag{11}$$

where V_u and the V_s are ultimate strength and strength corresponding to the first yielding, respectively. Therefore, over-strength is related to both V_u and V_s and they are discussed in the next section. Fig. 11 illustrates the over-strength versus t_f and ψ. As shown in this figure, Ω_0 is between 1.53 and 2.08, which is greater than the what the AISC suggests. Ji [27] also reported that the over-strength factors of very short shear links reached 1.9, significantly exceeding the value of 1.5 proposed by the AISC. This confirms the findings of the present study. The obtained value of Ω_0 is related to both h and t_f. For each h, by increasing t_f, Ω_0 is enhanced. The rate of increasing t_f concerning h is different. Therefore, Ω_0 for the FE simulation models was depicted versus ψ. There is no dimension factor that can be used for all types of dampers with different geometries. As shown in this figure, based on the fitting results, Eq. (12) is proposed to calculate Ω_0 for the proposed damper. This proposed equation is limited to $\psi < 16$.

Based on Eq. (10), the minimum value of Ω_0 is obtained in the range $8 \le \psi \le 12$. When $V_p < V_f$ the value of Ω_0 is large. Thus, it is suggested to design the damper with $V_p < V_f$.

5.5. Strength corresponding to the first yielding

In Table 4, the V_s of models is compared. Based on the results, by increasing h, V_s is reduced between 4% to 35%. By increasing t_f, V_s is reduced between 8% to 35%. Change in V_s for various values of h and t_f is not negligible. The values of V_s change irregularly for different h and t_f values; the relationship of V_s against ρ is depicted in Fig. 12.

Results indicate that V_p given by Eq. (1) does not predict V_s with high

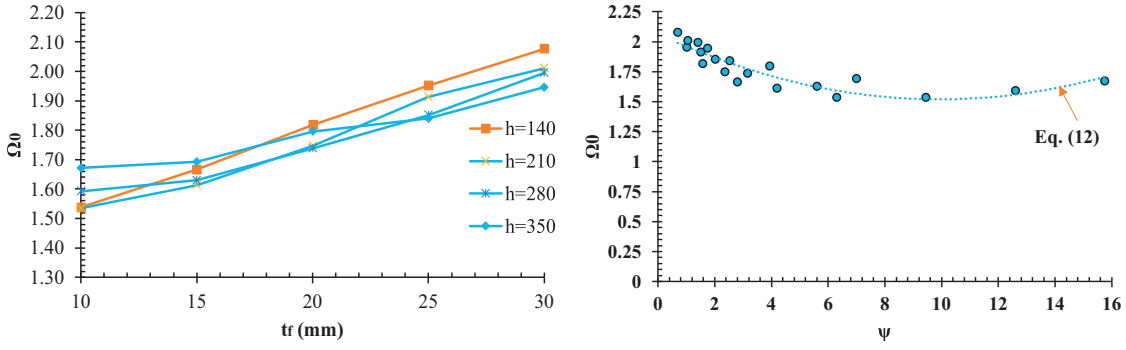

Fig. 11. Over-strength of the FE simulation models.

$$\Omega_0 = 0.0055\psi^2 - 0.11\psi + 2 \tag{12}$$

Table 4
Comparing strength corresponding to the first yielding for FE simulation models.

Models	ρ	ψ	t_f (mm)	Vs (kN)	$\frac{V_{s(i)}}{V_{s(h=140mm)}}$	$\frac{V_{s(i)}}{V_{s(t_f=10mm)}}$
140-10-0.25-6.3	0.25	6.30	10	315.251		
140-15-0.18-2.8	0.18	2.80	15	350.478	1.11	
140-20-0.13-1.58	0.13	1.58	20	400.107	1.27	
140-25-0.11-1.00	0.11	1.01	25	469.747	1.49	
140-30-0.10-0.7	0.09	0.70	30	556.27	1.76	
210-10-0.38-9.45	0.38	9.45	10	303.315		0.96
210-15-0.26-4.2	0.26	4.20	15	328.611	1.08	0.94
210-20-0.2-2.36	0.20	2.36	20	354.959	1.17	0.89
210-25-0.16-1.51	0.16	1.51	25	391.731	1.29	0.83
210-30-0.13-1.05	0.13	1.05	30	441.683	1.46	0.79
280-10-0.51-12.6	0.51	12.60	10	286.099		0.91
280-15-0.35-5.6	0.35	5.60	15	313.493	1.10	0.89
280-20-0.26-3.15	0.26	3.15	20	334.415	1.17	0.84
280-25-0.21-2.02	0.21	2.02	25	357.112	1.25	0.76
280-30-0.17-1.4	0.17	1.40	30	387.683	1.36	0.70
350-10-0.64-15.75	0.64	15.75	10	266.051		0.84
350-15-0.44-7.0	0.44	7.00	15	294.607	1.11	0.84
350-20-0.33-3.94	0.33	3.94	20	319.464	1.20	0.80
350-25-0.26-2.52	0.26	2.52	25	338.022	1.27	0.72
350-30-0.22-1.75	0.22	1.75	30	358.852	1.35	0.65

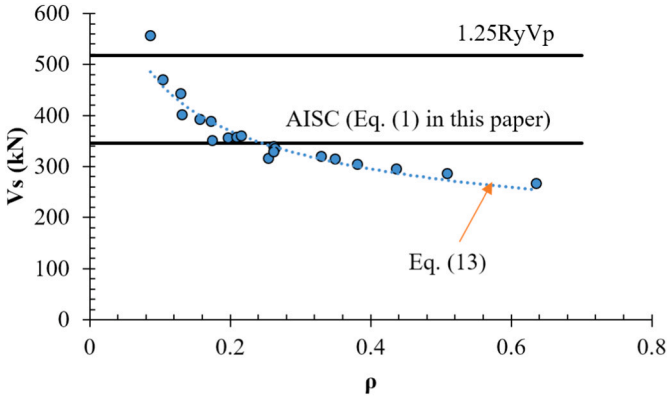

Fig. 12. Strength corresponding to the first yielding in the damper.

accuracy. Further, $1.25R_yV_p$ measures the upper bound of V_s. Therefore, V_p amplified by $1.25R_y$ cannot be used for predicting the ultimate strength of the link. The relationship for V_s is proposed in Eq. (13).

$$V_s = 220\rho^{-0.32} \tag{13}$$

6. Accuracy of the proposed relation

In Table 5, the results from FE modelling are compared with the values given by the proposed relations. In this table, Eq. (1) and (6) were used to calculate the ultimate strength according to the AISC presented in Section 2.3. Furthermore, Eq. (2) is the proposed relation from Section 2.3. It is evident that the proposed relations measure the ultimate strength of the I-shaped damper with high accuracy, with a maximum 3% error. Therefore, utilizing Eqs. (1) through Eq. (4), the proposed damper is designed; based on Eq. (5) through Eq. (13) the diagonal element brace is designed. The accuracy of the equations is measured in the next section.

Table 5
Accuracy of the proposed equations to determine ultimate strength of the damper.

Models	Ultimate strength (kN)				$\frac{Eq.(1)}{FE}$	$\frac{Eq.(6a)}{FE}$	$\frac{Eq.(2)}{FE}$
	FE	*Eq.* (1)	*Eq.* (6*a*)	Proposed formula-*Eq.* (2)			
140-10-0.25-6.3	484.76	346	518.4	435.02	0.71	1.07	0.99
140-15-0.18-2.8	583.88	346	518.4	520.87	0.59	0.89	0.98
140-20-0.13-1.58	727.55	346	518.4	634.15	0.48	0.71	0.96
140-25-0.11-1.00	917.02	346	518.4	774.86	0.38	0.57	0.93
140-30-0.10-0.7	1155.30	346	518.4	942.99	0.30	0.45	0.90
210-10-0.38-9.45	465.46	346	518.4	416.73	0.74	1.11	0.98
210-15-0.26-4.2	530.31	346	518.4	479.73	0.65	0.98	1.00
210-20-0.2-2.36	620.16	346	518.4	561.01	0.56	0.84	1.00
210-25-0.16-1.51	749.37	346	518.4	660.57	0.46	0.69	0.97
210-30-0.13-1.05	888.29	346	518.4	778.42	0.39	0.58	0.96
280-10-0.51-12.6	455.72	346	518.4	407.59	0.76	1.14	0.98
280-15-0.35-5.6	511.02	346	518.4	459.15	0.68	1.01	0.99
280-20-0.26-3.15	581.32	346	518.4	524.43	0.59	0.89	0.99
280-25-0.21-2.02	661.21	346	518.4	603.43	0.52	0.78	1.00
280-30-0.17-1.4	773.43	346	518.4	696.14	0.45	0.67	0.99
350-10-0.64-15.75	444.70	346	518.4	402.10	0.78	1.17	0.99
350-15-0.44-7.0	498.51	346	518.4	446.81	0.69	1.04	0.99
350-20-0.33-3.94	573.63	346	518.4	502.49	0.60	0.90	0.96
350-25-0.26-2.52	621.87	346	518.4	569.14	0.56	0.83	1.01
350-30-0.22-1.75	698.29	346	518.4	646.77	0.49	0.74	1.02

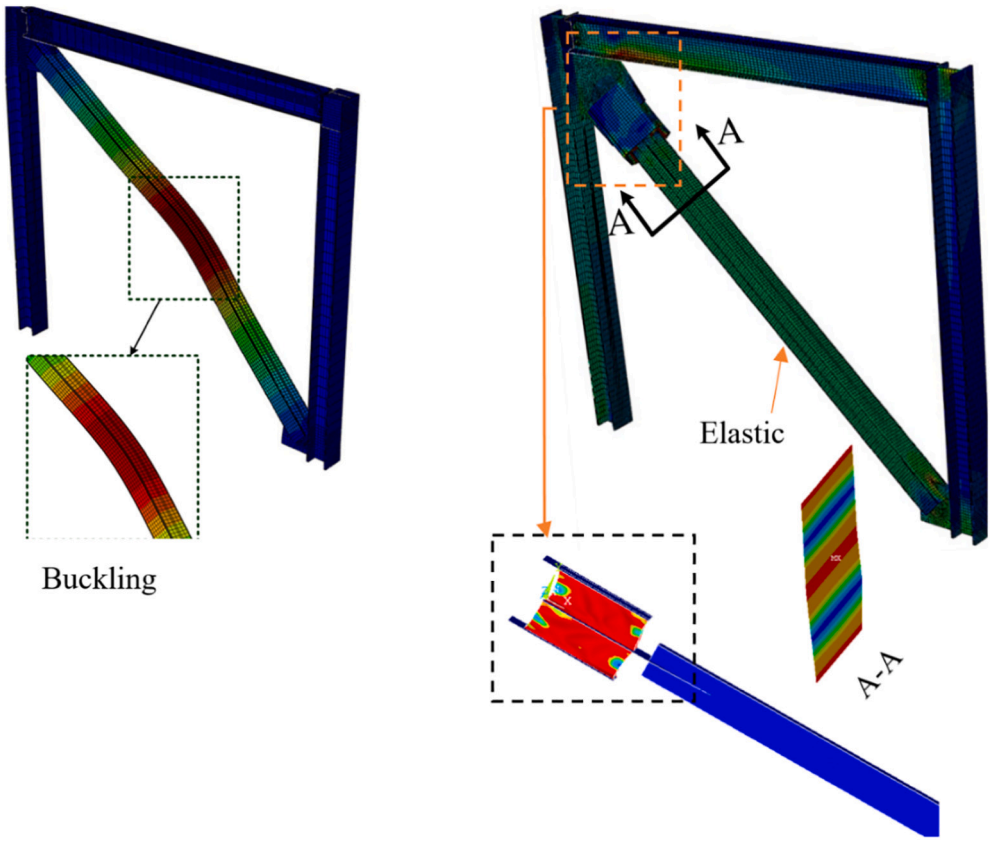

Fig. 13. Distributed stress over the system.

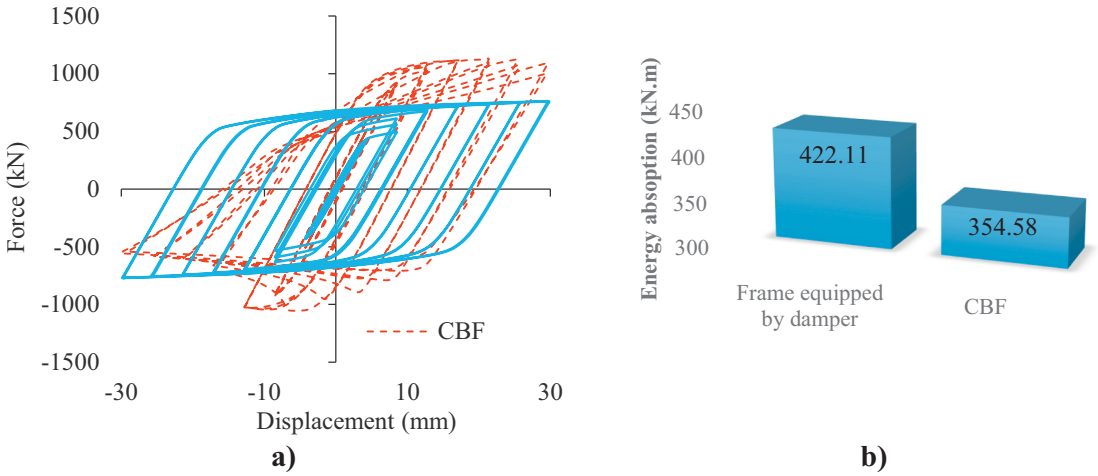

Fig. 14. Comparing the behaviour of CBF and CBF equipped with a damper.

7. Improving the diagonal brace member equipped with the proposed damper

To ensure suitable performance of proposed damper designed by the proposed relations, a diagonal brace equipped with the damper is evaluated in this section. To do so, a brace member was added to the damper with h = 140 mm. The brace was designed based on the Eqs. (7) to (11). In so doing, a frame with a height and length of 3 m was designed. For the CBF diagonal element, the 2UNP160 was selected. Further, IPE240 and IPB180 were used for the beam and columns. Since simple (pined) beam-to-column connection was considered, no lateral loading was carried by the frame.

The von Misses stress over the CBF and the CBF equipped by the damper is shown in Fig. 13. According to the figure, the diagonal element in the CBF system buckles, while it remains elastic when the damper is added. This confirms that the damper acts as a ductile fuse that prevents nonlinear behaviour of elements outside the damper.

In Fig. 14a, the hysteresis curves of the CBF and the CBF equipped by the damper are compared. For the plain CBF system, degradation in stiffness and strength can be observed, while no degradation is seen for the CBF equipped with the damper. The degradation of the hysteresis curve of the CBF under compression is due to the buckling of the bracing member. However, the ultimate strength of the CBF is greater than that of the system equipped with the damper; the energy dissipation of the

system without the damper is reduced by 16%, Fig. 13b.

8. Conclusions

In this study, an I-shaped shear link that acts as a damper was introduced and investigated numerically and parametrically. In addition, an equation required to design the damper was proposed. The findings are summarised as follows:

- Results indicate that a flange contributes to shear resistance of the I-shaped damper, 4% to 15%, while such a possibility is ignored in the AISC. Upon the formation of a shear hinge in the web plate, the plates begin to lose their effectiveness and frames become more active up to a rotation of 0.08 rad. After another rotation of 0.01 rad, the share of both flange and web plates is constant.
- By increasing h, ultimate strength is reduced, as long as $\rho < 1.6$ for all models. For dampers with $t_f = 10$ and 30 mm, ultimate strength is reduced for different values of h by 4% to 8% and 23% to 40%, respectively. Therefore, the reduction of V_u is higher for dampers with higher t_f. By increasing t_f while keeping h constant, ultimate strength is enhanced by 8% to 26%. Thus, the ultimate strength of the damper is not only related to ρ and ψ, it is also related to t_f and h.
- The over-strength Ω_0 is related to both h and t_f. For each h, if t_f increases, the value of Ω_0 also increases. The rate of increasing t_f for h is different.
- The minimum Ω_0 is obtained within the range $8 \leq \psi \leq 12$. When $V_p < V_f$ the value of Ω_0 is high. It is suggested to design the damper with $V_p < V_f$.
- By increasing h, V_s is reduced between 4% to 35%. By increasing t_f, V_s is reduced between 8% to 35%. The change in V_s for different values of h and t_f is not negligible.
- The proposed relation measures the ultimate strength of the damper with a maximum 3% error. The proposed relation is simple and is in high agreement with FE simulation results.
- Based on results, for the CBF system, the degradation in stiffness and strength have been observed while no degradation is seen in the CBF system equipped with the proposed damper. The degradation of the hysteresis curve of the CBF under compression is due to the buckling of the bracing member. However, the ultimate strength of the CBF is greater than that of the system equipped with the damper; the energy dissipation of the system without the damper is reduced by 16%.

Declaration of Competing Interest

The authors declare that they have no known competing financial interests or personal relationships that could have appeared to influence the work reported in this paper.

References

[1] K.D. Hjelmstad, E.P. Popov, "Seismic Behavior of Active Beam Link in Eccentrically Braced Frames." Rep. No. UCB/EERC-83/15, Earthquake Engineering Research Center, University of California, Berkeley, 1983.

[2] J.O. Malley, E.P. Popov, Shear links in eccentrically braced frames, J. Struct. Div. 110 (9) (1984) 2275–2295.

[3] K. Kasai, E.P. Popov, "A Study of Seismically Resistant Eccentrically Braced 418 Frames." Rep. No. UCB/EERC-86/01, Earthquake Engineering Research Center, University of California, Berkeley, 1986.

[4] M.D. Engelhardt, E.P. Popov, "Behavior of Long Links in Eccentrically Braced Frames." Rep. No. UCB/EERC-89/01, Earthquake Engineering Research Center, University of California, Berkeley, 1989.

[5] E.P. Popov, M.D. Engelhardt, Seismic eccentrically braced frames, J. Constr. Steel Res. 10 (1988) 321–354.

[6] T. Okazaki, G. Arce, H.C. Ryu, M.D. Engelhardt, Experimental study of 431 local buckling, overstrength, and fracture of links in eccentrically braced frames, J. Struct. 432 Eng. 131 (10) (2005) 1526–1535, 433.

[7] T. Okazaki, M.D. Engelhardt, Cyclic loading behavior of EBF links 434 constructed of ASTM A992 steel, J. Constr. Steel Res. 63 (6) (2007) 751–765, 435.

[8] T. Okazaki, M.D. Engelhardt, A. Drolias, E. Schell, J.K. Hong, C.M. Uang, Experimental investigation of link-to-column connections in eccentrically braced frames, J. Constr. Steel Res. 65 (7) (2009) 1401–1412.

[9] M.D. Engelhardt, E.P. Popov, Experimental performance of long links in eccentrically braced frames, J. Struct. Eng. (ASCE) 118 (11) (1992) 3067–3088.

[10] V. Mohsenian, I. Hajirasouliha, R. Filizadeh, Seismic reliability analysis of steel moment-resisting frames retrofitted by vertical link elements using combined series–parallel system approach, Bull. Earthq. Eng. 19 (2021) 831–862, https://doi.org/10.1007/s10518-020-01013-9.

[11] G. Della Corte, M. D'Aniello, R. Landolfo, Analytical and numerical study of plastic overstrength of shear links, J. Constr. Steel Res. 82 (2013) 19–32.

[12] X. Ji, Y. Wang, Q. Ma, T. Okazaki, Cyclic behavior of very short steel shear links, J. Struct. Eng. (ASCE) 142 (2) (2015), 04015114.

[13] A. Chesoan, A. Stratan, D. Dubina, Design implementation of re-centring dual eccentrically braced frames with removable links, Soil Dyn. Earthq. Eng. 112 (2018) 174–184.

[14] M.B. Bozkurt, C. Topkaya, Replaceable links with gusseted brace joints for eccentrically braced frames, Soil Dyn. Earthq. Eng. 115 (2018) 305–318.

[15] M.G. Vetr, A. Ghamari, Experimentally and analytically study on eccentrically braced frame with vertical shear links, Struct. Design Tall Spec. Build. 28 (5) (2019), e1587, https://doi.org/10.1002/tal.1587.

[16] M. Seki, H. Katsumata, H. Uchida, T. Takeda, Study on Earthquake Response of Two-Storied Steel Frame with Y-shaped Braces. Proceedings 9th World Conference on Earthquake Engineering, Tokyo-Kyoto, Japan, 1988, pp. 65–70.

[17] M.R. Baradaran, F. Hamzezarghani, M. RastegariGhiri, Z. Mirsanjari, The effect of vertical shear-link in improving the seismic performance of structures with eccentrically bracing systems, Int. J. Civil Environ. Eng. 9 (8) (2015) 1078–1082.

[18] J. Bouwkamp, M.G. Vetr, A. Ghamari, An analytical model for inelastic cyclic response of eccentrically braced frame with vertical shear link (V-EBF), Case Stud. Struct. Eng. 6 (2016) 31–44.

[19] A. Ghadami, Gh. Pourmoosavi, A. Ghamari, Seismic design of elements outside of the short low-yield-point steel shear links, J. Constr. Steel Res. 178 (2021), https://doi.org/10.1016/j.jcsr.2020.106489.

[20] V. Mohsenian, A. Nikkhoo, Evaluation of performance and seismic parameters of eccentrically braced frames equipped with dual vertical links, StructEngMech 69 (6) (2019) 591–605.

[21] Jack Bouwkamp, Mohamad Ghasem Vetr, Ali Ghamari, An analytical model for inelastic cyclic response of eccentrically braced frame with vertical shear link (V-EBF), Case Stud. Struct. Eng. 6 (2016) 31–44, https://doi.org/10.1016/j.csse.2016.05.002.

[22] AISC, AISC 341–16, Seismic Provisions for Structural Steel Buildings, American Institute of Steel Construction, Chicago, IL, USA, 2016.

[23] ANSI/AISC 360-16, Specification for structural steel buildings, Inst. Steel Constr. Am. (2016) 1–612.

[24] C.C. McDaniel, C.M. Uang, F. Seible, Cyclic testing of built-up steel shear links for the new bay bridge, J. Struct. Eng. ASCE 129 (6) (2003) 801–809.

[25] D.N. Manheim, E.P. Popov, Plastic shear hinges in steel frames, J. Struct. Eng. ASCE 109 (10) (1983) 2404–2419.

[26] P.W. Richards, Cyclic Stability and Capacity Design of Steel Eccentrically Braced Frames (Ph.D. Thesis) Department of Structural Engineering, University of California, San Diego, San Diego, CA, 2004.

[27] X. Ji, Y. Wang, Q. Ma, T. Okazaki, Cyclic behavior of very short steel shear links, J. Struct. Eng. 142 (2) (2016) 04015114, https://doi.org/10.1061/(ASCE)ST.1943-541X.0001375.